Computational Analysis of a Passive Wake Alleviation Scheme

Gregory J. McCauley[*]   Philip S. Marcus[†]

Ömer Savaş[‡]

University of California at Berkeley, Berkeley, California, 94720-1740

Donald A. Durston[§]

NASA Ames Research Center, Moffett Field, California, 94035-1000

The vortex wake generated by a large aircraft induces sizeable vertical forces and rolling moments on trailing aircraft during an encounter. Recent studies of wake alleviation have focused on experimental observations of both active and passive techniques for accelerating the breakdown of the vortical structures in these wakes through vortex instabilities. A subset of these studies have concentrated on the addition of outboard triangular flaps for passively inciting Crow-like instabilities in the trailing vortices. Accompanying computational studies have been limited to qualitative analyzes of the general wake features and vortex breakdown. To help bridge the quantitative gap between experimental and computational results, a spectral Navier-Stokes simulation was used to analyze the evolution of the vortical structures in the wake to calculate the forces and rolling moments induced on a trailing wing. Significant reductions in both downwash and rolling moment are clearly present in the numerical work; the magnitude and time scale of these reductions correlate well with recent experimental studies.

Nomenclature

b^*	centroid span
b_f	following wing span
b_t	wing span
c_f	chord length of trailing planform
d	flap span
r_{EN}	radius of enstrophy
t	time
$\mathbf{u}$	velocity vector
v	vertical velocity induced by generating planform
x', y'	transformed coordinates with origin at center of trailing planform
$\mathbf{x}_{EN}$	enstrophy centroid
$C_{l\alpha_f}$	two-dimensional lift-curve slope

---

[*]Graduate Student, Department of Mechanical Engineering; gregmc@me.berkeley.edu, Student Member AIAA.

[†]Professor, Department of Mechanical Engineering; pmarcus@me.berkeley.edu

[‡]Professor, Department of Mechanical Engineering; savas@me.berkeley.edu, Associate Fellow AIAA.

[§]Aerospace Engineer, Experimental Aero-Physics Branch; Don.Durston@nasa.gov, Senior Member AIAA.

American Institute of Aeronautics and Astronautics

D	downwash
EN	enstrophy
L	mapping parameter for computational domain
L_y	lift of trailing planform
M_y	moment about y-axis on trailing planform
R	rolling moment on trailing planform
Re_Γ	circulation-based Reynolds number, Γ_{tot}/ν
T	orbital period
T_{b*}	downwash period
U	speed of generating planform
U_0	velocity of trailing planform
χ	toroidal velocity component
ν	kinematic viscosity
ω	vorticity
ψ	polodial velocity component
ρ	density
σ_f	flap vortex core radius
σ_t	tip vortex core radius
Γ_f	flap circulation
Γ_H	circulation of horseshoe vortex
Γ_t	wing circulation
Γ_{tot}	circulation of half wing
$\oplus$	vorticity centroid

Subscripts

exp	experimental measurement
num	numerical value

I.   Introduction

The trailing vortex wakes induced by large aircraft pose a significant hazard to following aircraft. During an encounter with a wake, a trailing aircraft may experience sizeable vertical and rolling forces which can lead to a loss of control. During takeoff and landing, the proximity of the ground increases the danger of control loss. Furthermore, the fixed flight corridors instituted by airports exacerbate the issue by enforcing similar paths for both leading and following aircraft. To reduce the probability of wake encounters, minimum separation distances are enforced between aircraft during takeoff and landing, which significantly limit the capacity of an airport. While these separation distances are conservative, they do not guarantee safe flight since the dissipation of the vortices has a significant dependence on atmospheric conditions, which can shift the position of the vortices or impede the natural breakdown of the coherent vortical wake structure. A recent perspective of the problem and further resources may be found in the *Dossier* complied by Crouch and Jacquin[1] and the references therein.

This natural breakdown is caused by the induction and subsequent amplification of the Crow instability, a sinus perturbation that ultimately leads to the formation of vortex rings from the initially parallel wake vortices.[2] Before the instability erodes the coherence of the trailing wake structure, however, the well-formed vortical features present in the wake may influence the motion of trailing craft for several nautical miles behind the generating aircraft. This natural instability provided the initial seed for a class of methods to reduce the risk of wake vortex encounters.

Two methodologies have been proposed to reduce the likelihood of catastrophic control loss while allowing reduced separation distances, thereby enhancing the efficiency of impacted airports. One methodology involves tracking the evolution of the wake vortices induced by a leading aircraft, allowing trailing craft to

American Institute of Aeronautics and Astronautics

successfully navigate around the vortical structures present in the wake. While this approach shows promise, some conditions, including atmospheric winds and measurement limitations, currently restrict its practical application. Atmospheric winds, which can change direction and speed rapidly, may reposition the wake vortices sporadically, leading to wake encounters for aircraft which were previously clear of the hazard. In addition, such shifts in vortex position, coupled with the variance of atmospheric conditions, require greater scope and accuracy than is offered by current measurement techniques, which are inadequate even in calm conditions.

The second methodology seeks to modify the wake of the leading aircraft to reduce its coherence downstream and thereby reduce its impact on following aircraft. While many approaches have been tested, few led to pronounced acceleration of the wake vortex breakdown. It should be noted, however, that early studies may not have investigated a parameter space large enough to encompass configurations which would ultimately lead to wake vortex alleviation and so should not necessarily be discarded without further analysis.[3] Thus far, the methods with the greatest promise for achieving accelerated incoherence in the trailing wake rely upon inciting Crow-like instabilities in the wake rather than allowing these perturbations to form over the natural time scale.

The excitation of Crow-like instabilities to force wake breakdown may be further subcategorized into active and passive methods. Active techniques typically rely upon oscillation of the wing loading to introduce Crow-like perturbations into the wake. These oscillations may result from the deployment of wing flaps, movement of control surfaces, and flexure of the wing surface in a periodic manner. Due to their reliance on physical oscillations that may ultimately lead to structural fatigue, the implementation of active schemes may be hindered by regulatory commissions or maintenance requirements. In contrast, passive techniques rely upon a fixed wing loading to induce the requisite instabilities. These methods often incorporate the wing into the design process, reshaping it to create the vortex structure necessary to incite Crow-like perturbations. Unfortunately, current passive alleviation schemes exhibit notable structural or aerodynamic penalties which render this approach challenging on existing aircraft, even impractical. However, the extension of this technique to six- or eight- vortex systems may allow these penalties to be redistributed or reduced. Since this avenue remains available, passive techniques may offer a built-in solution for future aircraft without the need for active control mechanisms.

A four-vortex wake generated by rectangular wings with outboard triangular flaps emerged from tow tank experiments at Berkeley as a passive scheme for wake alleviation.[4–6] The alleviation characteristic of this wake was studied using flow visualization and particle image velocimetry. Later, Haverkamp et al. and Durston et al. verified the results independently and extended the parameters covered by the experimental studies.[7,8] The results of these studies indicated a substantial increase in the three-dimensionality of the wake, and thus a loss of overall coherence, over a substantially shorter time span than the natural time scale. A remarkable feature of the work by Durston et al. was the use of wing-tail configurations to achieve wake structures similar to the outboard-flapped wing, while offering a less intrusive modification to current aircraft. Concurrent numerical studies by Bristol et al., confirmed the qualitative results observed during the experiments of the triangular-flapped wing.[9] Using a spectral Navier-Stokes solver, simulations of the far-field wake led to vortex decay in an analogous manner. More recently, Winckelmans et al. found similar qualitative results using a hybrid vortex method, though due to the relatively low circulation-based Reynolds number, it is unclear how to draw a direct comparison to the aforementioned experimental results.[10,11]

To further investigate the four-vortex wake flow and in preparation for extensions to six- or eight-vortex systems, a numerical study of the wake alleviation aspects of the vortex system is undertaken here. The problem is outlined in Figure 1. The figure shows sketches of the two-vortex wake behind a rectangular wing (left column) and the four-vortex wake behind an outboard triangular-flapped wing (right column). The wing planforms are shown in (c). Lift distributions (a) and their derivatives (b) are calculated from a finite wing analysis for planar wings, hence the curvature effects of the wings used in experiments are not included. Vortex sheet roll up is sketched in (d). The far-field wake vortex structure is shown in (e). The vorticity centroids for each half of the wings are marked. Reference system is defined in (e). Note that an overall vorticity centroid for a finite wing is undefined. A summary of the numerical technique is presented

American Institute of Aeronautics and Astronautics

first. A set of measures for characterization of a vortex wake is presented next. The remainder of the paper discusses numerical results and makes comparisons to the experiments of Ortega et al.[4,5]

II.   Numerical Method

The computational fluid dynamics (CFD) code used for the current study is a spectral Navier-Stokes solver developed by Matsushima and Marcus.[12–14] This package employs rational Legendre functions which are algebraically mapped to the radial coordinate and periodic basis functions in both the axial and azimuthal directions to represent a cylindrical-polar investigation domain (Figure 2). The formulation of this numerical method satisfies the pole condition exactly, in spite of the coordinate singularity, and alleviates the stiffness issues often introduced by this singular region. The dissipation of energy at small length scales is enforced by a simple hyperviscosity model.

The velocity field $\mathbf{u}$, which is assumed to be divergence-free, is decomposed into toroidal ψ and poloidal χ components

$$\mathbf{u} = \nabla \times (\mathbf{e}_z \psi) + \nabla \times \nabla \times (\mathbf{e}_z \chi), \tag{1}$$

and is initialized using

$$\mathbf{u} \cdot \mathbf{e}_z = -\nabla_\perp^2 \chi \tag{2}$$

$$\omega \cdot \mathbf{e}_z = \nabla_\perp^2 \psi. \tag{3}$$

For all simulations presented herein, the vorticity field is initialized by centering a Gaussian vorticity distribution at each vortex core location. The Gaussian vorticity distribution, or Lamb-Oseen vortex, is chosen for its good correlation with experimentally-observed wake vortices.[15] The tip vortices are given initial strengths of $\Gamma_t = 2\pi$. The core radii of the outer and inner vortices are $\sigma_t = 0.0628b_t$ and $\sigma_f = 0.677\sigma_t$, respectively, to approximate the average of the experimentally-observed ratios. The span between the tip vortices is set to $b_t = 16$ and the dynamic viscosity is chosen as $\nu = 1 \times 10^{-4}$ to achieve the same order of the circulation-based Reynolds number Re_Γ as observed experimentally. To incite the evolution of the wake structure, the inboard vortices are perturbed by a sinusoidal displacement with amplitude of $0.01\sigma_f$ and wavelength of $4b_t$. The hyperviscosity coefficient is initialized as one-third of the dynamic viscosity.

To maximize the resolution of the spectral method in the investigation region, both the center of the computational domain and the mapping parameter L for the Legendre polynomials are varied for each data set. During initialization, the centroid of vorticity is relocated to the center of the computational domain (Figure 4). Furthermore, the mapping parameter is set to 2.5 or 2 times the radial distance from the centroid to the outermost vortex core edge for half- and full-wing simulations, respectively. An additional factor of $\sqrt{2}$ is allocated for data cropping.

The integral quantities for downwash and rolling moment are evaluated throughout the entire flow field output by the CFD program, and the maximal downwash and rolling moment are used as a measure of the vortex wake coherence. As the distance between the tip and flap vortices varies along the length of the perturbation wavelength, variations in vorticity, downwash, and rolling moment are expected, certainly during the maturing stages of the amplification. To determine the magnitude of these variations, the quantities of interest are sampled on four equally-spaced planes 1-4 along the first quarter of the wavelength (Figures 2). Since wake vortices pose a greater hazard to smaller aircraft, the span of the following wing b_f is chosen to be half that of the generating planform. It should be noted that due to the finite span of the wing, a region of $b_f/2$ provides insufficient data for integration and must be discarded from both the left and right sides of the velocity field.

A.   Wake Characterization

This study will focus on the simulation and analysis of the far-field wake, where the vortex sheet generated by the wing has rolled up into discrete vortices. The resulting wake structures consist of two equal-strength

American Institute of Aeronautics and Astronautics

counter-rotating vortices for a rectangular wing and two pairs of unequal-strength counter-rotating vortices for the triangular-flapped planform (Figure 1). It should be noted that, due to the effects of vortex sheet rolling, the span b_t between the tip vortices of strength Γ_t and the distance d measured from the tip vortices to flap vortices of strength Γ_f vary slightly from similar wing parameters. For the purposes of scaling, a centroid of vorticity with circulation $\Gamma_{tot} = \Gamma_t - \Gamma_f$ can be defined for each half of the wing and marked as $\oplus$ in Figure 1.

1. Vorticity Distribution

After Ortega et al.,[5] we will use enstrophy to describe the distribution of vorticity in the wake, which avoids difficulties in describing a vorticity distribution when the vorticity is not all of the same sign. We will use $\omega^2 = \omega_x^2 + \omega_y^2 + \omega_z^2$ to indicate the complete definition of enstrophy when all three components of the vector are avaliable as in the case of the CFD calculations, and use only ω_z^2 for the vorticity along the z-axis when data is available in one plane only, as is the case with experiments. The total enstrophy EN is determined as

$$EN = \int \omega^2 dA \qquad (4)$$

and the position of the enstrophy centroid, $\mathbf{x}_{EN} = (x_{EN}, x_{EN})$, from

$$\mathbf{x}_{EN} = \frac{1}{EN} \int \mathbf{x} \omega^2 dA. \qquad (5)$$

For an equi-strength counter-rotating vortex pair, the enstrophy centroid is at the midpoint of the vortices while the vorticity centroid is undefined. We will use the enstrophy dispersion radius r_{EN} defined as

$$r_{EN}^2 = \frac{1}{EN} \int |\mathbf{x} - \mathbf{x}_{EN}|^2 \omega^2 dA \qquad (6)$$

to describe the extent of the spread of vorticity in the flow. Similar calculations are carried out for EN_z based on ω_z^2.

2. Downwash and Rolling Moment

Previous experimental investigations used the forces and moments experienced by a following wing as an effective measure of wake vortex hazard. In early studies, direct measurements were typically taken by flying a smaller plane through the wake of a larger aircraft. Due to safety and monetary constraints, these large scale efforts were later disbanded for models and wings towed in the wake of a generating aircraft. The experiments of Ortega et al. further simplified this approach by using the velocity induced by a generating airfoil to deduce the forces experienced by a smaller trailing wing, an idea which was proposed earlier by Rossow.[5,16]

Following Rossow and Ortega et al.,[5,16] the lift experienced by a following rectangular wing of span b_f (Figure 3) is

$$L_y = \frac{1}{2} C_{l\alpha_f} \rho U_0^2 c_f \int_{-b_f/2}^{b_f/2} \frac{v(x', y')}{U_0} dx'. \qquad (7)$$

The trailing aircraft speed U_0 will be assumed equal to the generating aircraft speed U and the average integral quantity

$$D = -\frac{1}{b_f} \int_{-b_f/2}^{b_f/2} v(x', y') dx' \qquad (8)$$

will be used as a surrogate for the downwash for subsequent analyses.[4] It should be noted that the downwash above is the negative of that presented by Ortega et al. This choice enforces the sense of positive downwash

American Institute of Aeronautics and Astronautics

as imposing a force toward the ground. Furthermore, the axes have been transformed to coincide with those used in the computational domain. Similarly, the induced rolling moment is

$$M_y = \frac{1}{2} C_{l\alpha_f} \rho U_0^2 c_f \int_{-b_f/2}^{b_f/2} x' \frac{v(x', y')}{U_0} dx'. \tag{9}$$

Again, only the average integral quantity

$$R = \frac{1}{b_f} \int_{-b_f/2}^{b_f/2} x' v(x', y') dx' \tag{10}$$

will be considered.

3. Scaling

For the direct comparison of the various numerical and experimental results, a set of time, force, and moment scalings is necessary. The orbital period of two vortices, given by

$$T = \frac{4\pi^2 d^2}{\Gamma_{tot}} \tag{11}$$

is appropriate for comparisons of different four-vortex wakes. It is, however, inadequate for temporal comparisons between the complete wakes induced by rectangular and triangular-flapped wings, since Γ_{tot} vanishes. Instead, the period it takes for the vorticity centroids to traverse a centroid span b^* downwards is employed. This period

$$T_{b^*} = \frac{2\pi \left(b^*\right)^2}{\Gamma_{tot}} \tag{12}$$

will be referred to as the downwash period. This temporal scaling allows the consideration of two- and four-vortex wake evolutions and can be related to the downstream coordinate

$$\frac{z(t)}{b} = \frac{T_{b^*,exp}}{T_{b^*,num}} \frac{U_{exp}}{b_{exp}} t_{num} \tag{13}$$

used by Ortega et al. and Durston et al.[4,8]

For comparison of the downwash and rolling moment between two- and four-vortex wakes, a simple horseshoe vortex model of the wing is used to estimate the total lift of the planform.[4] The lift for each wing, which is proportional to $U\Gamma_{tot}b^*$, is equated to the lift for a single horseshoe vortex of strength Γ_H and span b_t. Solving for the circulation of the bound horseshoe vortex provides

$$\Gamma_H = \left(\frac{b^*}{b_t}\right) \Gamma_{tot}. \tag{14}$$

III.   Lamb-Oseen Vortex

To validate the quantitative aspects of both the original numerical code, as well as the modifications necessary to calculate the induced downwash and rolling moment, a comparison of the analytical solution and numerical output of the flow induced by an isolated Lamb-Oseen vortex is carried out. The azimuthal velocity distribution for a Lamb-Oseen vortex of size σ is

$$u_\theta = \frac{\Gamma}{2\pi r} \left(1 - e^{-r^2/\sigma^2}\right) \tag{15}$$

American Institute of Aeronautics and Astronautics

and its vorticity distribution

$$\omega_z = \frac{\Gamma}{\pi\sigma^2} e^{-r^2/\sigma^2}. \tag{16}$$

The downwash for the vortex can be calculated from Equation 8

$$D = -\frac{\Gamma}{2\pi b_f} \int_{-b_f/2}^{b_f/2} \frac{x'}{r^2} \left[1 - e^{-r^2/\sigma^2} \right] dx' \tag{17}$$

and the rolling moment from Equation 10

$$R = \frac{\Gamma}{2\pi b_f} \int_{-b_f/2}^{b_f/2} \frac{(x')^2}{r^2} \left[1 - e^{-r^2/\sigma^2} \right] dx'. \tag{18}$$

which are evaluated numerically and shown in Figure 5. As expected, the extreme values of the downwash occur on either side of the vortex and the maximum rolling moment at its center. The results from the CFD output are identical to the analytical solution in Equations 17 and 18.

IV. Vortex Wake Simulations

The vortex wake induced by a triangular-flapped wing consists of two sets of counter-rotating vortices (Figure 1). The wake is parameterized using the flap-wing span ratio d/b_t and the tip-flap vortex strength ratios Γ_f/Γ_t. The calculation for $(\Gamma_f/\Gamma_t, d/b_t) = (-0.37, 0.25)$ is shown in Figures 6-10 and discussed extensively below. The calculation is for the full wing span and corresponds to the experiment photographed in Figure 4 of Ortega et al.[5] and to a similar calculation shown in Figure 16 of Bristol et al.[9]

The evolution of the wake in Figure 6 is visualized using an isosurface of the vorticity magnitude at $0.174\omega_{max} = 0.167\frac{\Gamma_t}{\pi\sigma_t^2}$. The sinusoidal perturbations of the flap vortices grow rapidly due to the strain field induced by the stronger tip vortices. The sinus perturbations become clearly noticeable by $t/T = 1$ and pairs evidently become incoherent by $t/T = 2$. As the vortex pairs on each side of the wing begin to merge, the Ω-loops observed in previous studies begin to form.[5,9,11] For the calculations presented here, these loops do not form rings and cross the wake as observed in the experimental studies. However, this behavior was observed previously using the same spectral code with a significantly higher hyperviscosity coefficient.[9]

Figure 7 is a snapshot of the wake at $t/T = 1.1$ while the perturbations are still at their infancy and Figure 8 at $t/T = 2.2$ by which time the vortex pairs have lost their coherence (c.f. Figure 6). In both figures, the first column shows the vorticity distribution, the second the downwash, and the third the rolling moment. The rows in the figures (also in Figures 9 and 10 below) correspond to the sampling planes 1-4 marked in Figure 2. The vortical structure of the wake is coherent at $t/T = 1.1$ and does not exhibit a comparable organized structure. The two halves of the wake, however, remain distinct.

Figure 9 shows the evolution of enstrophy. The right column shows both the enstrophy and the enstrophy dispersion radius based on ω^2 and the left column based on ω_z^2. Using either measure, the enstrophy shows an abrupt change around $t/T = 2$. Enstrophy EN or EN_z shows a sudden increase followed by a gradual decrease. During this time, the dispersion radii show oscillations at about the orbital frequency, corresponding to the orbiting motion of the vortices. As the instabilities breakdown the wake, these oscillations cease, and the radii increase. If the radii calculations were carried out for half of the wake only, they would exhibit a low plateau followed by a sharp rise in phase with EN (see Figure 16 below).

The maximum values of downwash and rolling moment are shown in Figure 10. Initially, downwash shows a periodic variation with period T and rolling moment with period $T/2$. Clearly, simultaneous with the enstrophy, the downwash and rolling moment take sharp turns downward at about $t/T = 2$. Downwash falls by about $1/2$ and rolling moment by $2/3$. This sharp decrease is the direct consequence of the loss of coherence of the vortex wake as seen in the figures above.

For comparison, a series of calculations were carried out for circulation ratios of $\Gamma_f/\Gamma_t = 0.20, 0.30, 0.40,$ 0.50, 0.60 and separation distances of $d/b_t = 0.50, 0.625, 0.75, 0.825$. These calculations were done over

American Institute of Aeronautics and Astronautics

the half wing span, rather than the full wing span and carried out for five or more orbital periods. This is done for expedience, but not without justifications. For the parameters of interest, the vortex pairs on either side of the wing are sufficiently far apart that their mutual interaction is small, as demonstrated by previous calculations (Bristol et al. p.342,[9]) and by sample calculations done during the course of this study. Therefore, these simulations should provide a basis for the full wing simulations.

In these calculations, while the majority of the downwash and rolling moment evolution curves indicate a significant decrease in both quantities after 2-5 orbital periods (Figures 11,12), a few cases exhibit no significant alleviation (Figures 13,14). For these types of wake structures, the contours have a form similar to those of the isolated Lamb-Oseen vortex (*c.f.* Figure 5) over the entire simulation period. These instances typically maintain a strong core of vorticity, probably due to a relatively weak interactions between vortices.

The enstrophy data on the four planes in Figures 9 are averaged and presented in Figure 15. There seem to be no significant differences between the average and individual histories of enstrophy. The enstrophy results calculated for the half-wake from the full-wing simulation data are shown in Figure 16 to facilitate direct comparison with the PIV measurements of Ortega et al.[5] This averaging was done since the location of the PIV data plane with respect to instability waves in the experiments is unknown. Measurements and calculations show remarkably similar behavior, rapid transitions nearly at the same time and of comparable magnitudes. Slight variations in time shift can be easily compensated by injecting into calculations slightly different initial perturbation amplitudes. Similarly, the downwash, and rolling moment data on the four planes in Figure 10 are averaged and presented in Figure 17 for comparison with the results of Ortega et al.[4] The magnitude of the marked decrease in both downwash and rolling moment and the time over which these reductions occur are almost indistinguishable.

V.   Conclusions

The spectral CFD study presented here accurately predicts integral properties of a four-vortex wake proposed as solution for wake alleviation. The rolling moment and downwash fields are similar in both numerical and experimental studies and the trend of accelerated wake alleviation occurs in a similar manner in both studies. The magnitudes of both experimental and numerical values correlate well, though the time scale of the computational studies is slightly longer than that observed in the experimental work. This discrepancy is most likely due to the small perturbation size chosen for during initialization of the problem and can be corrected in future work. Furthermore, the choice of a significantly lower hyperviscosity coefficient than in previous studies is apparent in the evolution of the vorticity isosurfaces, as indicated by the diffuse vorticity present after merger. Comparison of the two- and three-dimensional wake structure results from the CFD simulation to two-dimensional measurements establishes that the PIV measurements are adequate to capture the salient features of the flow, hence can characterize the vortex wake well. This spectral vortex code offers a suitable platform to investigate six- and eight-vortex systems without incurring the cost of parameterized experimental studies. Thus, future experimental works can be steered by numerical studies of wake structures which show the most promise for accelerated wake alleviation.

References

[1]Crouch, J. and Jacquin, L., "Aircraft Trailing Vortices," *Comptes Rendus Physique*, Vol. 6, May 2005, pp. 392–582.

[2]Crow, S. C., "Stability theory for a pair of trailing wakes," *AIAA Journal*, Vol. 8, 1970, pp. 2172–2179.

[3]Savaş, O., "Experimental investigations on wake vortices and their alleviation," *Comptes Rendus Physique*, Vol. 6, Nov. 2005, pp. 415–429.

[4]Ortega, J. M., Bristol, R. L., and Savaş, O., "Wake Alleviation Properties of Triangular-Flapped Wings," *AIAA Journal*, Vol. 40, No. 4, 2002, pp. 709–721.

[5]Ortega, J. M., Bristol, R. L., and Savaş, O., "Experimental Study of the Instability of Unequal-Strength Counter-Rotating

Vortex Pairs," *Journal of Fluid Mechanics*, Vol. 474, Jan. 2003, pp. 35–84.

[6]Bristol, R. L., Ortega, J. M., and Savaş, O., "Experimental study of corotating wake-vortex merger at Reynolds numbers of order 10^5," *AIAA Journal*, Vol. 41, No. 4, April 2003, pp. 741–744.

[7]Haverkamp, S., Neuwerth, G., and Jacob, D., "Studies on the influence of outboard flaps on the vortex wake of a rectangular wing," *Aerospace Science and Technology*, Vol. 7, No. 5, July 2003, pp. 331–339.

[8]Durston, D. A., Walker, S. M., Driver, D. M., Smith, S. C., and Savaş, O., "Wake Vortex Alleviation Flow Field Studies," *Journal of Aircraft*, Vol. 42, No. 4, 2005, pp. 894–907.

[9]Bristol, R. L., Ortega, J. M., Marcus, P. S., and Savaş, O., "On Cooperative Instabilities of Parallel Vortex Pairs," *Journal of Fluid Mechanics*, Vol. 517, Oct. 2004, pp. 331–358.

[10]Winckelmans, G. S., "Vortex Methods," *Comptes Rendus Physique*, Vol. 6, Nov. 2005, pp. 467–486.

[11]Winckelmans, G. S., Cocle, R., Dufresne, L., and Capart, R., "Vortex methods and their application to trailing wake vortex simulations," *Comptes Rendus Physique*, Vol. 6, Nov. 2005, pp. 467–486.

[12]Matsushima, T. and Marcus, P. S., *Spectral methods in polar coordinates with an application to the stability of a trailing vortex wake*, Ph.D. thesis, University of California at Berkeley, California, 1995.

[13]Matsushima, T. and Marcus, P. S., "A spectral method for polar coordinates," *Journal of Computational Physics*, Vol. 120, 1995, pp. 365–374.

[14]Matsushima, T. and Marcus, P. S., "A spectral method for unbounded domains," *Journal of Computational Physics*, Vol. 137, 1997, pp. 321–345.

[15]Chen, A., Jacob, J., and Savaş, O., "Dynamics of Corotating Vortex Pairs in the Wakes of Flapped Airfoils," *Journal of Fluid Mechanics*, Vol. 383, 1999, pp. 155–193.

[16]Rossow, V. J., "Lift-Generated Vortex Wakes of Subsonic Transport Aircraft," *Progress in Aerospace Sciences*, Vol. 35, No. 6, 1999, pp. 507–660.

American Institute of Aeronautics and Astronautics
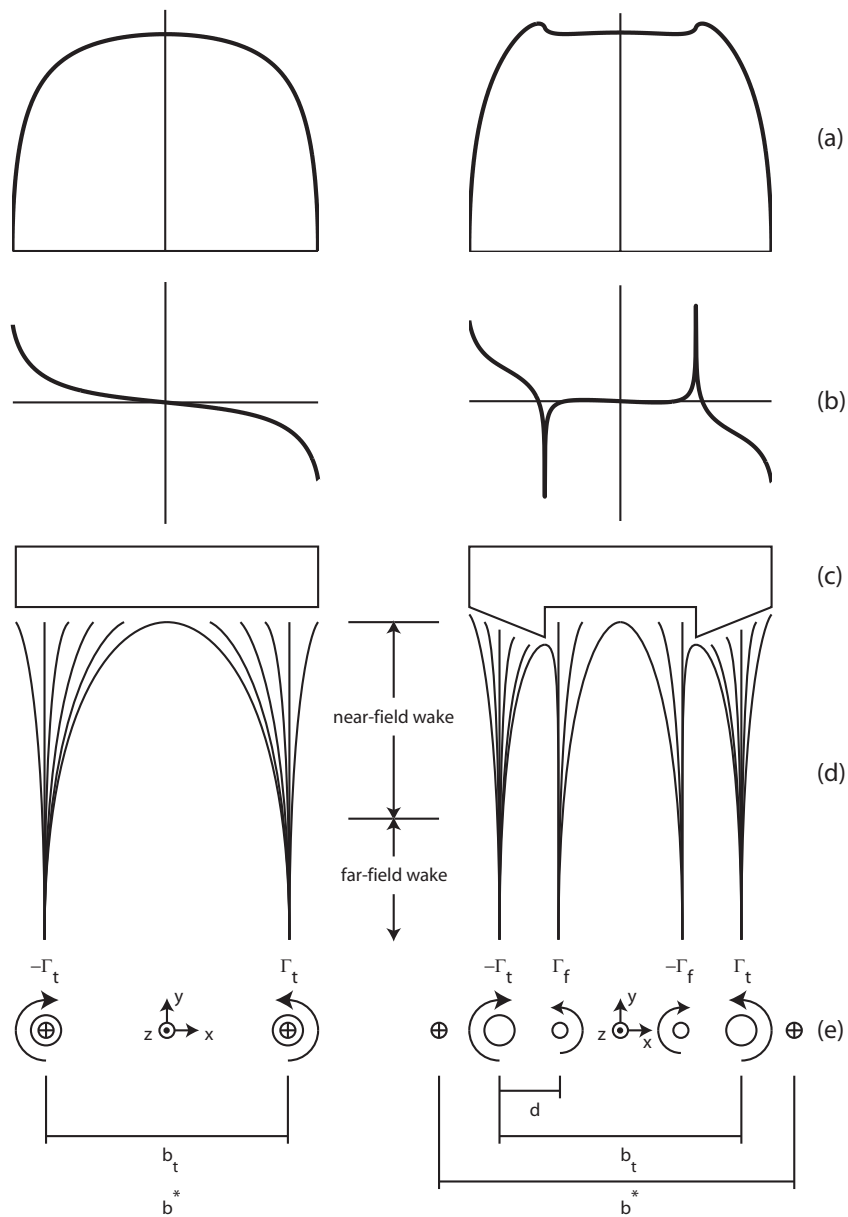
Figure 1. Sketches of the vortex wake evolution behind a rectangular (left column) and an outboard triangular-flapped (right column) wing planforms shown in (c). Lift distributions are shown in (a) and their derivatives in (b). Vortex sheet roll up is sketched in (d). The far-field wake vortex structure is shown in (e). The vorticity centroids for each half of the wings are marked by ⊕.

American Institute of Aeronautics and Astronautics
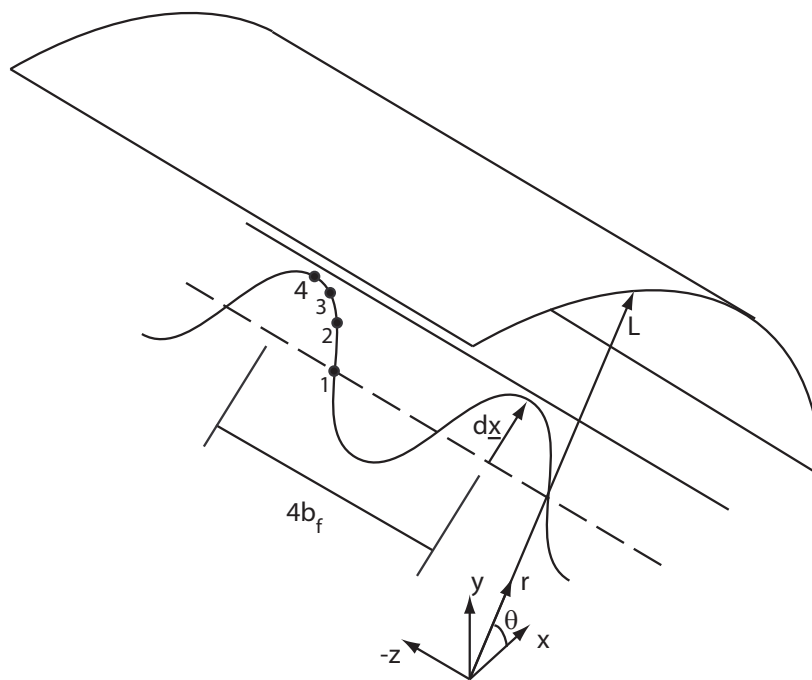
Figure 2. Cylindrical-polar domain used for the computational study. The partial cylindrical surface represents the separation between low- and high-detail regions and is determined by the mapping parameter L. Computational results are sampled at equispaced planes 1-4 marked as • along the initial perturbation cycle.

American Institute of Aeronautics and Astronautics
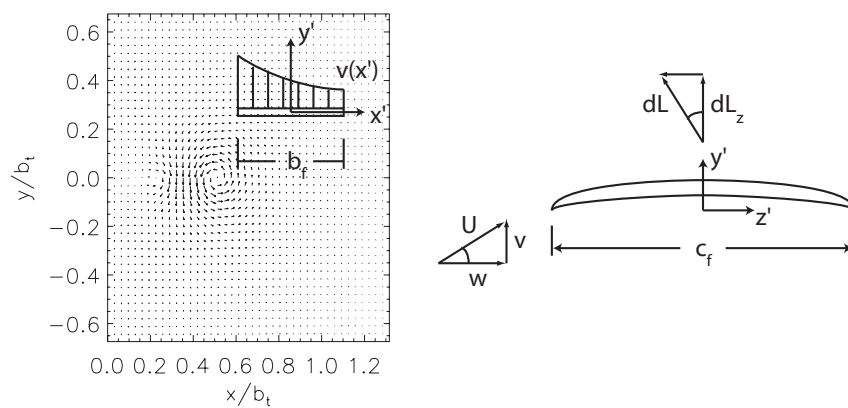
Figure 3. Schematic of a following wing in the velocity field induced by a outboard triangular-flapped planform (left) and a cross section of the flow about the following wing (right).[4]
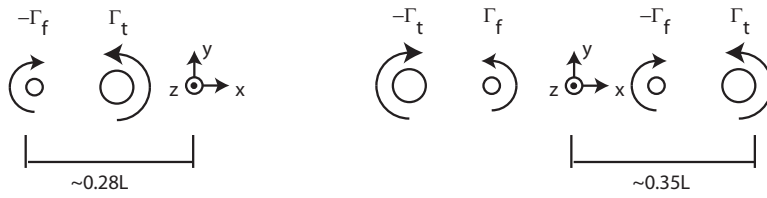
Figure 4. Domain initialization for the simulation of a half-wing (left) and a full-wing (right).
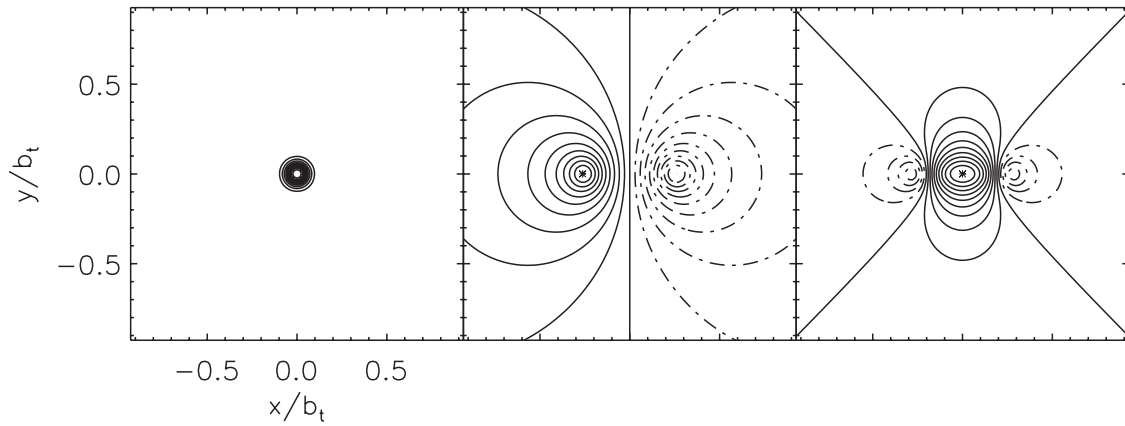
Figure 5. Vorticity (left), induced downwash (center), and rolling moment (right) of a Lamb-Oseen vortex. Numerical and analytical calculations are indistinguishable. The extreme values for downwash and rolling moment are each indicated by an *.

American Institute of Aeronautics and Astronautics

t/T = 0.00   t/T = 0.22

t/T = 0.44   t/T = 0.66

t/T = 0.88   t/T = 1.10

t/T = 1.32   t/T = 1.54

t/T = 1.76   t/T = 1.98
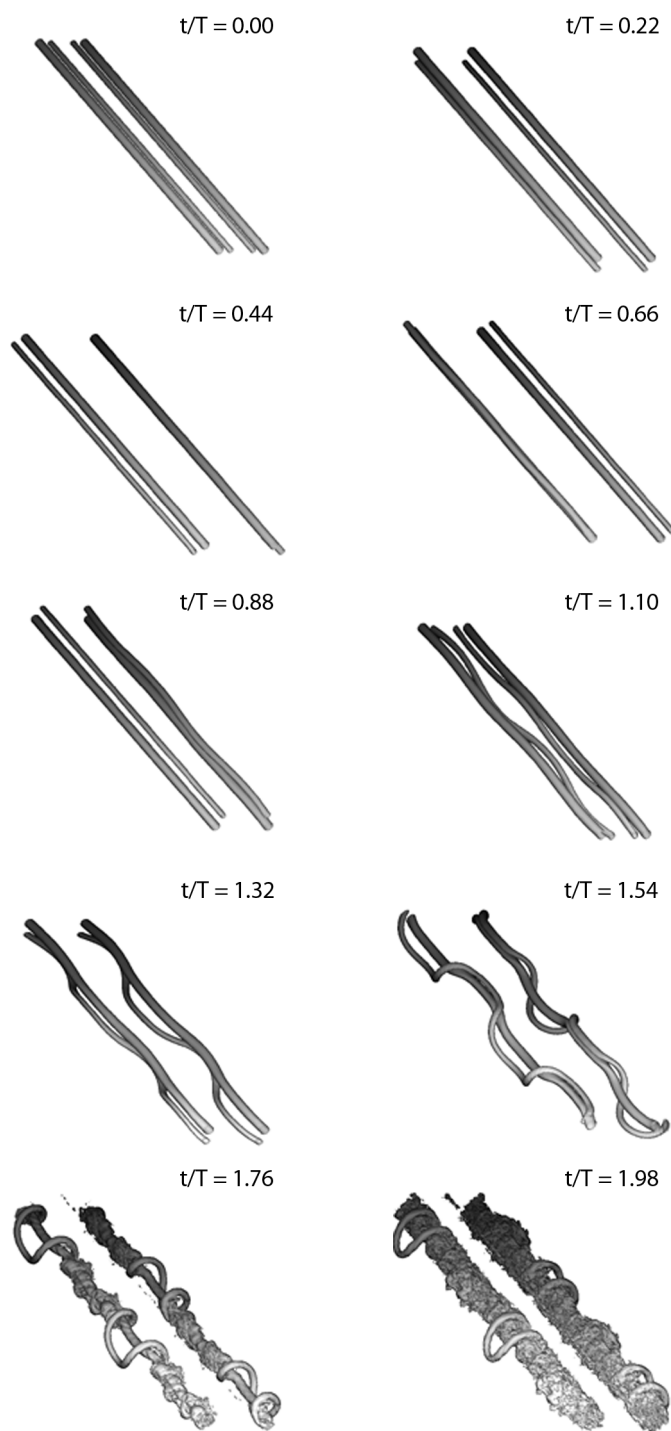
Figure 6. An oblique view of the wake evolution for a four vortex system with $\Gamma_f/\Gamma_t = -0.37$ and $d/b_t = 0.25$. Isosurfaces mark vorticity modulus of $0.174\omega_{max} = 0.167\frac{\Gamma_f}{\pi\sigma_f^2}$.
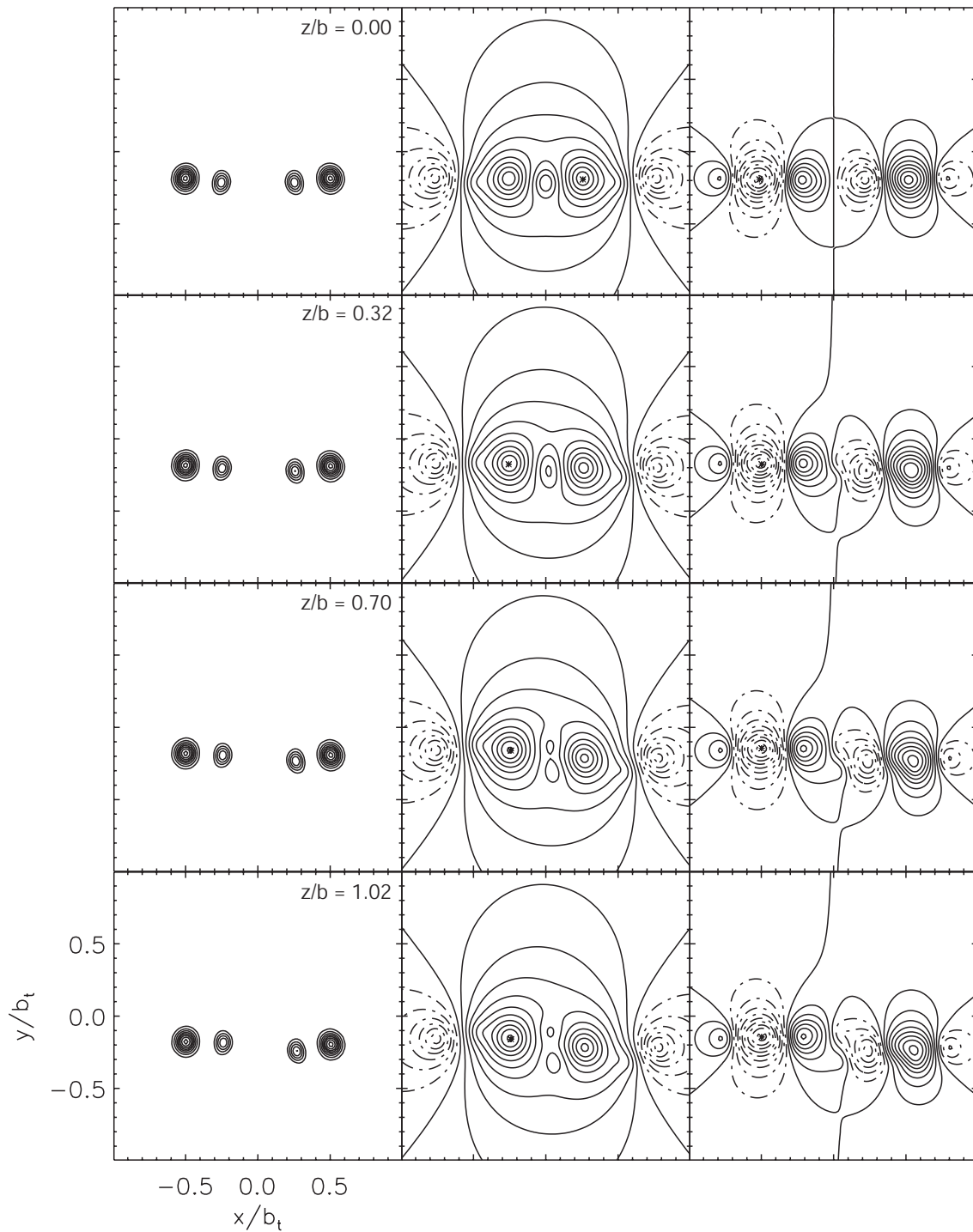
Figure 7. Vorticity (left), downwash (center), and rolling moment (right) induced by a two-vortex system with $\Gamma_f/\Gamma_t = -0.37$ and $d/b_t = 0.25$ at $z/b_t = 0,\ 0.3,\ 0.7,\ 1$ from top to bottom. Contours are drawn at $t/T = 1.1$ and are equally-spaced between the absolute values of the initial maximal values.

American Institute of Aeronautics and Astronautics
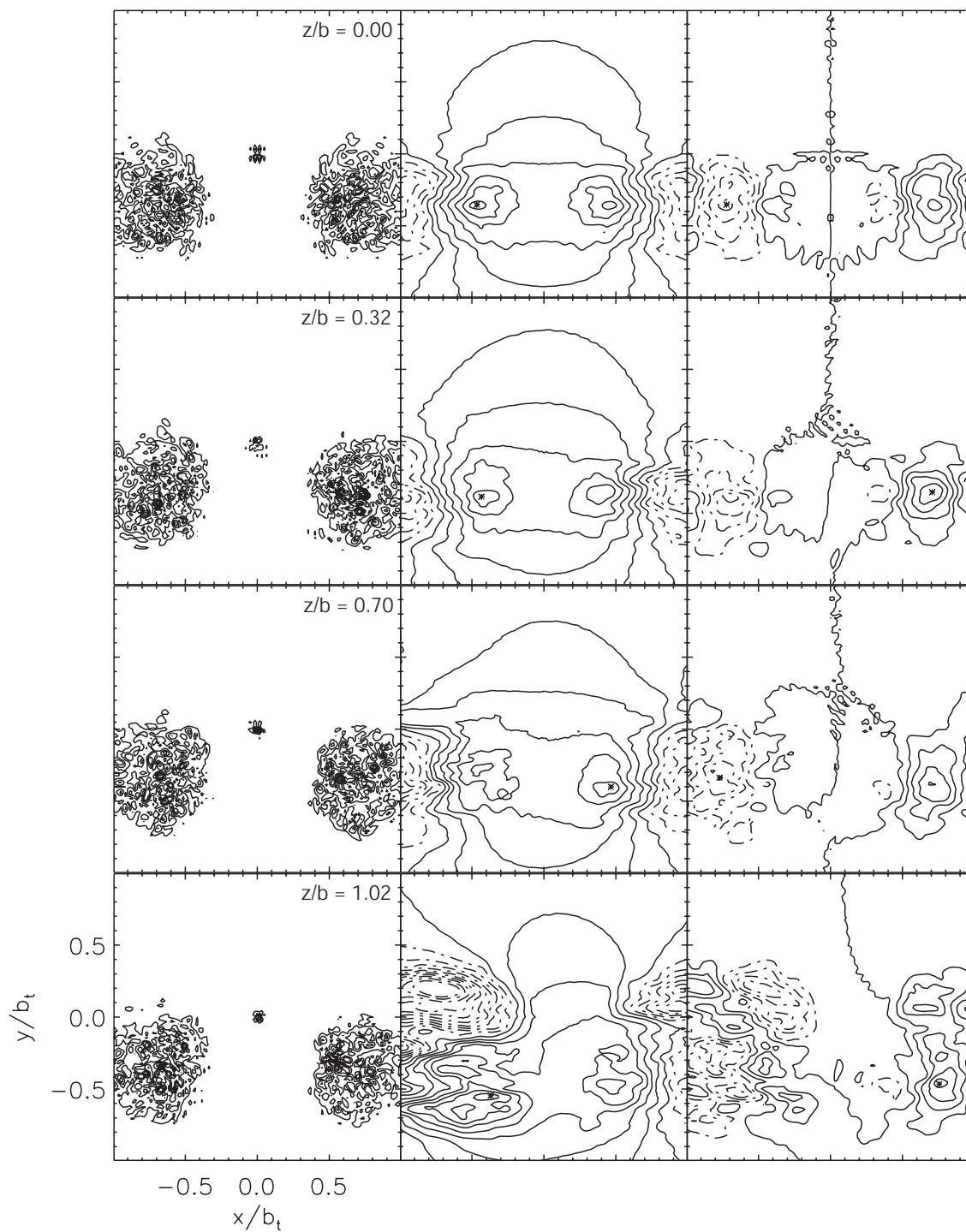
Figure 8. Vorticity (left), downwash (center), and rolling moment (right) induced by a two-vortex system with $\Gamma_f/\Gamma_t = -0.37$ **and** $d/b_t = 0.25$ **at** $z/b_t = 0,\ 0.3,\ 0.7,\ 1$ **from top to bottom. Contours are drawn at** $t/T = 2.2$ **and are equally-spaced between the absolute values of the initial maximal values.**

American Institute of Aeronautics and Astronautics
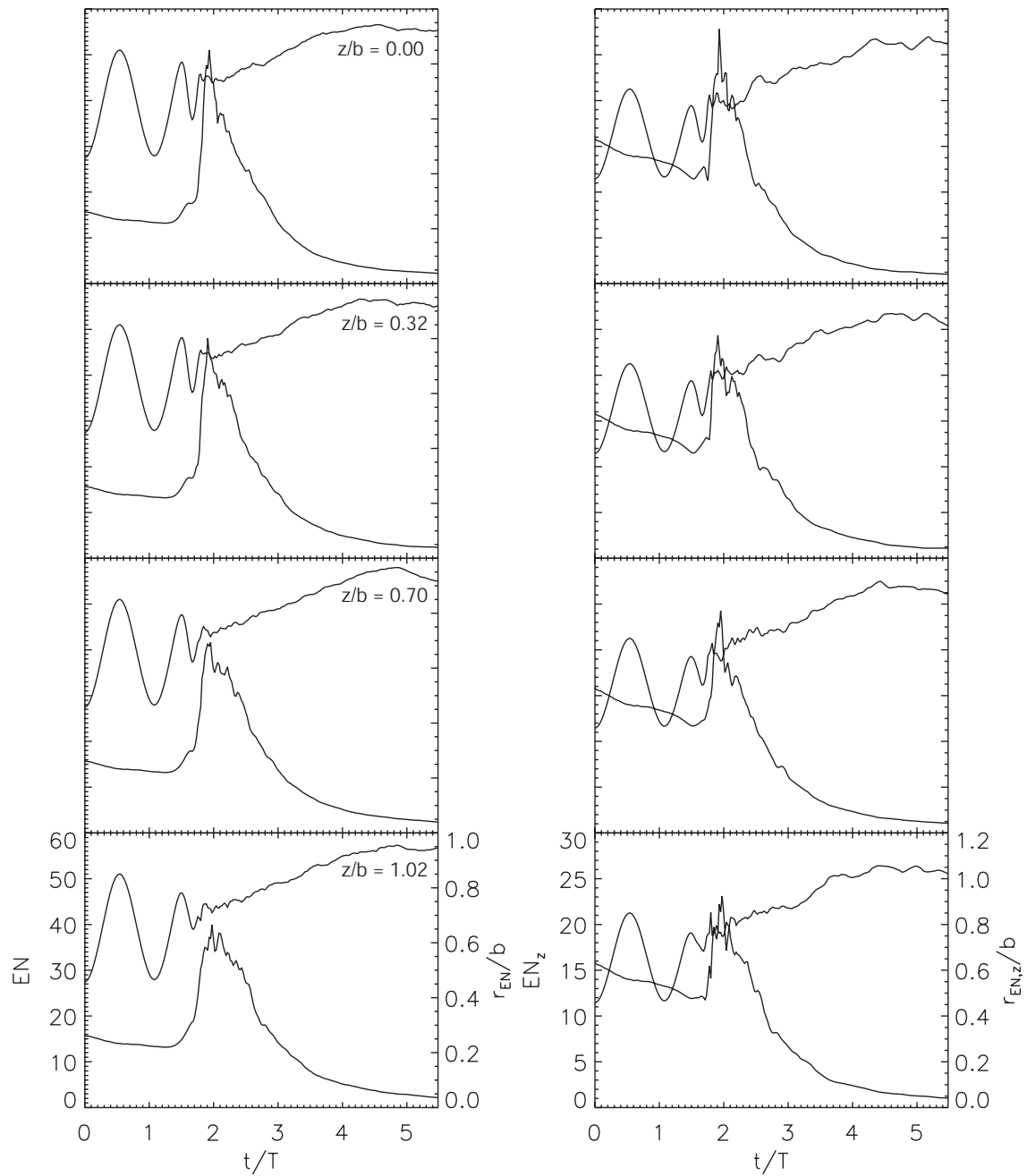
Figure 9. **Evolution of enstrophy for $\Gamma_f/\Gamma_t = -0.37$ and $d/b_t = 0.25$: (left) of total vorticity $\omega^2 = \omega_x^2 + \omega_y^2 + \omega_z^2$ and (right) of axial vorticity component ω_z^2. Both enstrophy and enstrophy dispersion radii are shown.**

American Institute of Aeronautics and Astronautics
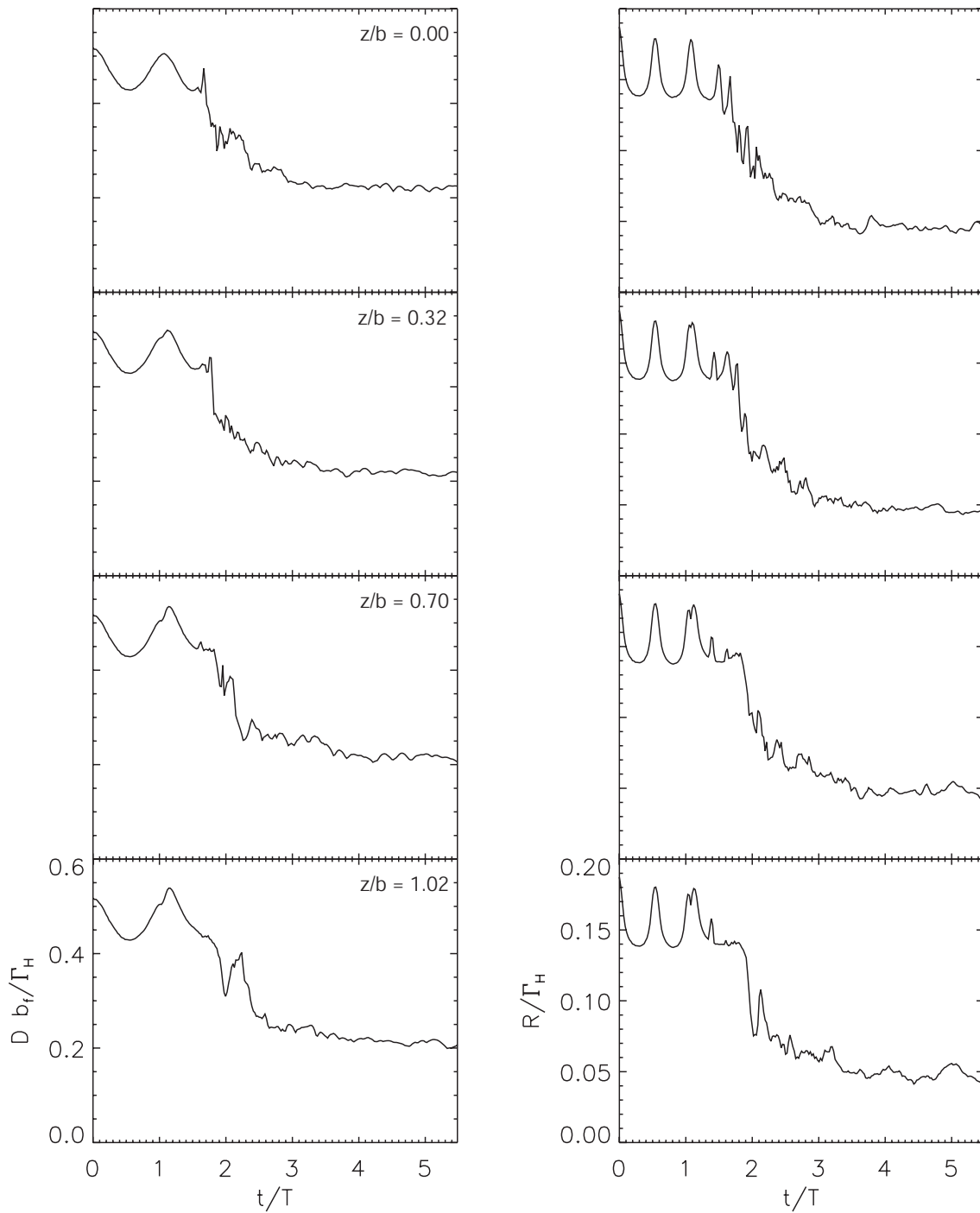
Figure 10. Peak values of downwash (left) and rolling moment (right) evolution incited by a two-vortex system with $\Gamma_f/\Gamma_t = -0.37$ and $d/b_t = 0.25$ at different axial planes.

American Institute of Aeronautics and Astronautics
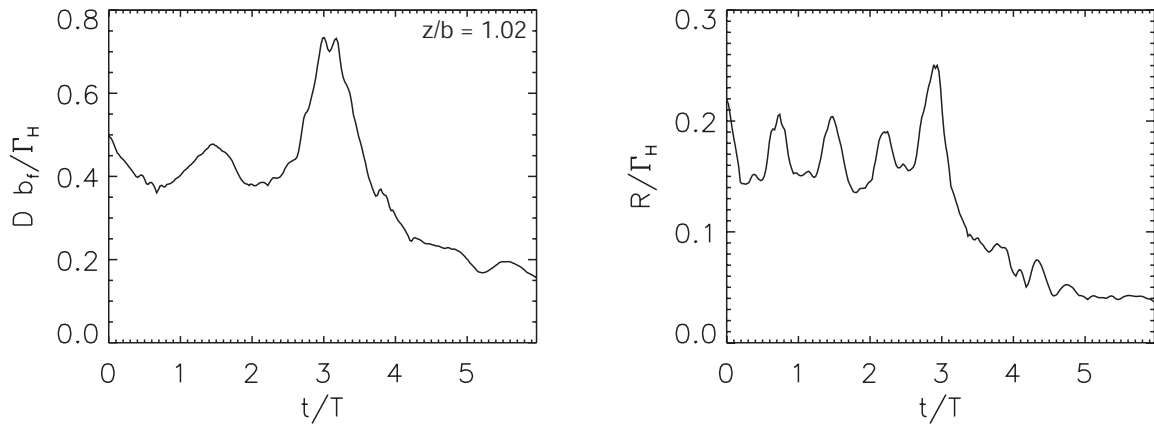
Figure 11. A significant increase in downwash (left) or rolling moment (right) is possible during merger as indicated by the evolution curves for a two-vortex system with $\Gamma_f/\Gamma_t = -0.60$ and $d/b_t = 0.125$ on the $z/b_t = 1.02$ plane.

American Institute of Aeronautics and Astronautics
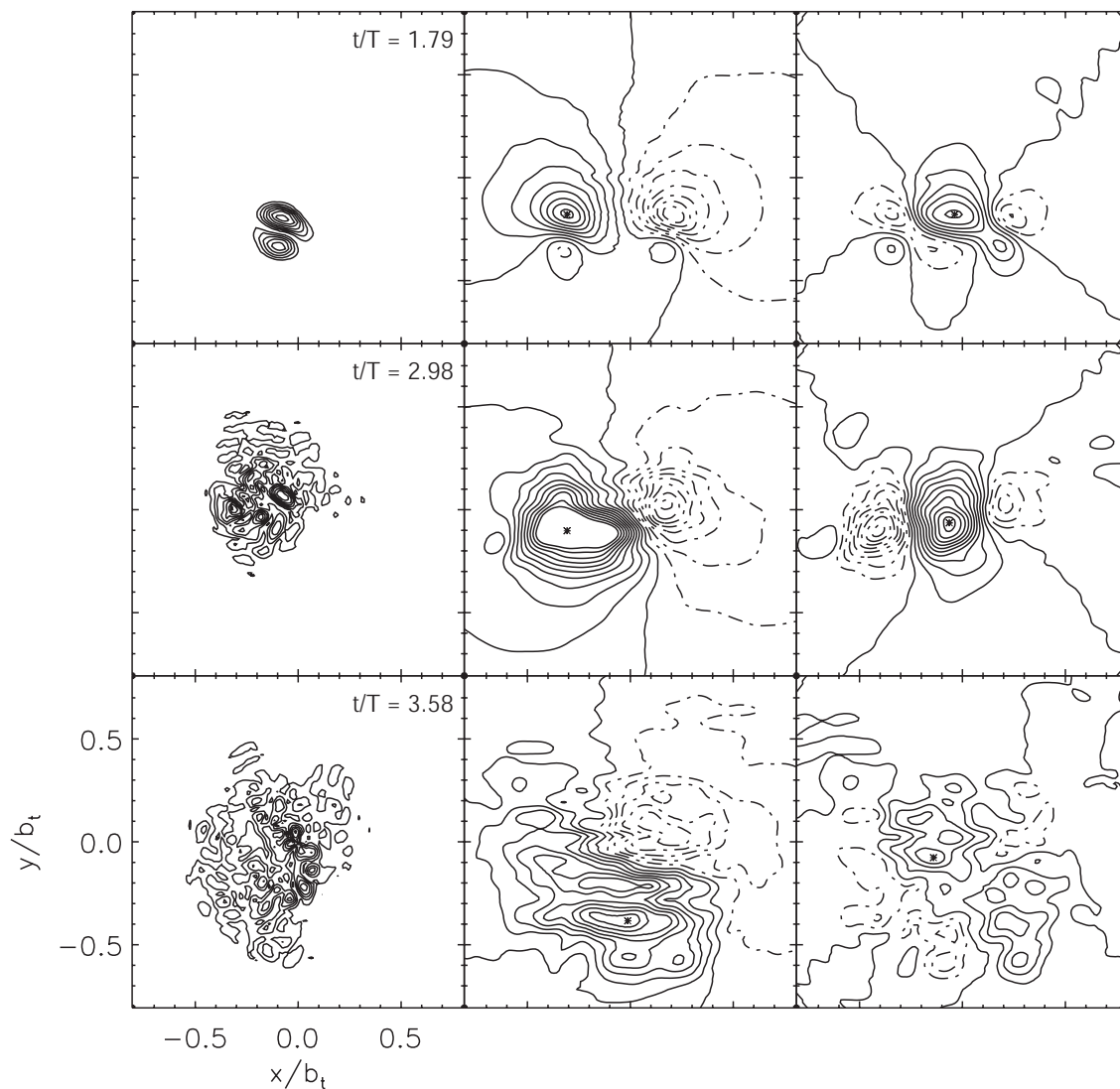
Figure 12. Vorticity (left), downwash (center), and rolling moment (right) contours for a two-vortex system with $\Gamma_f/\Gamma_t = -0.60$ and $d/b_t = 0.125$ sampled at plane 4 indicated in Figure 2. Contours are equally-spaced between the absolute values of the initial maximal values.

American Institute of Aeronautics and Astronautics
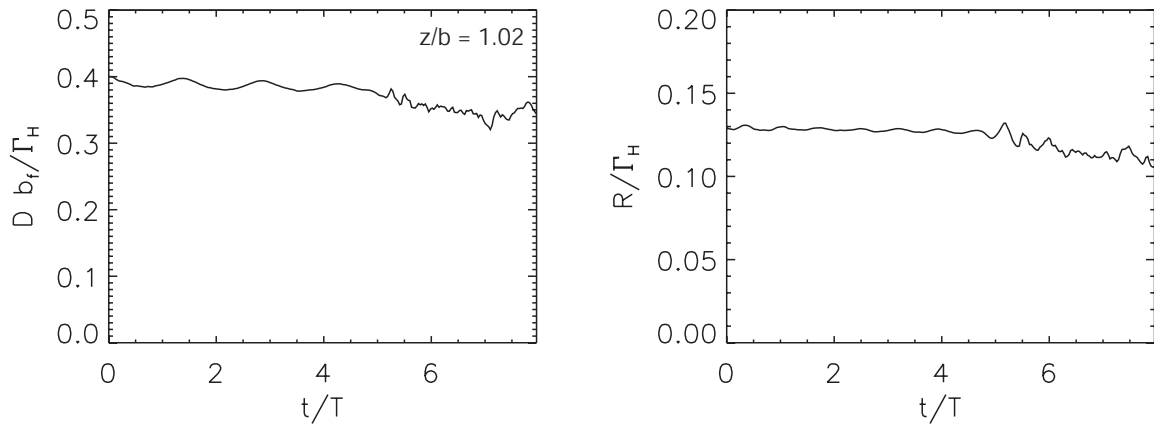
Figure 13. The downwash (left) and rolling moment (right) are not necessarily alleviated by the introduction of a flap vortex, as illustrated by a two-vortex system with $\Gamma_f/\Gamma_t = -0.20$ and $d/b_t = 0.125$.
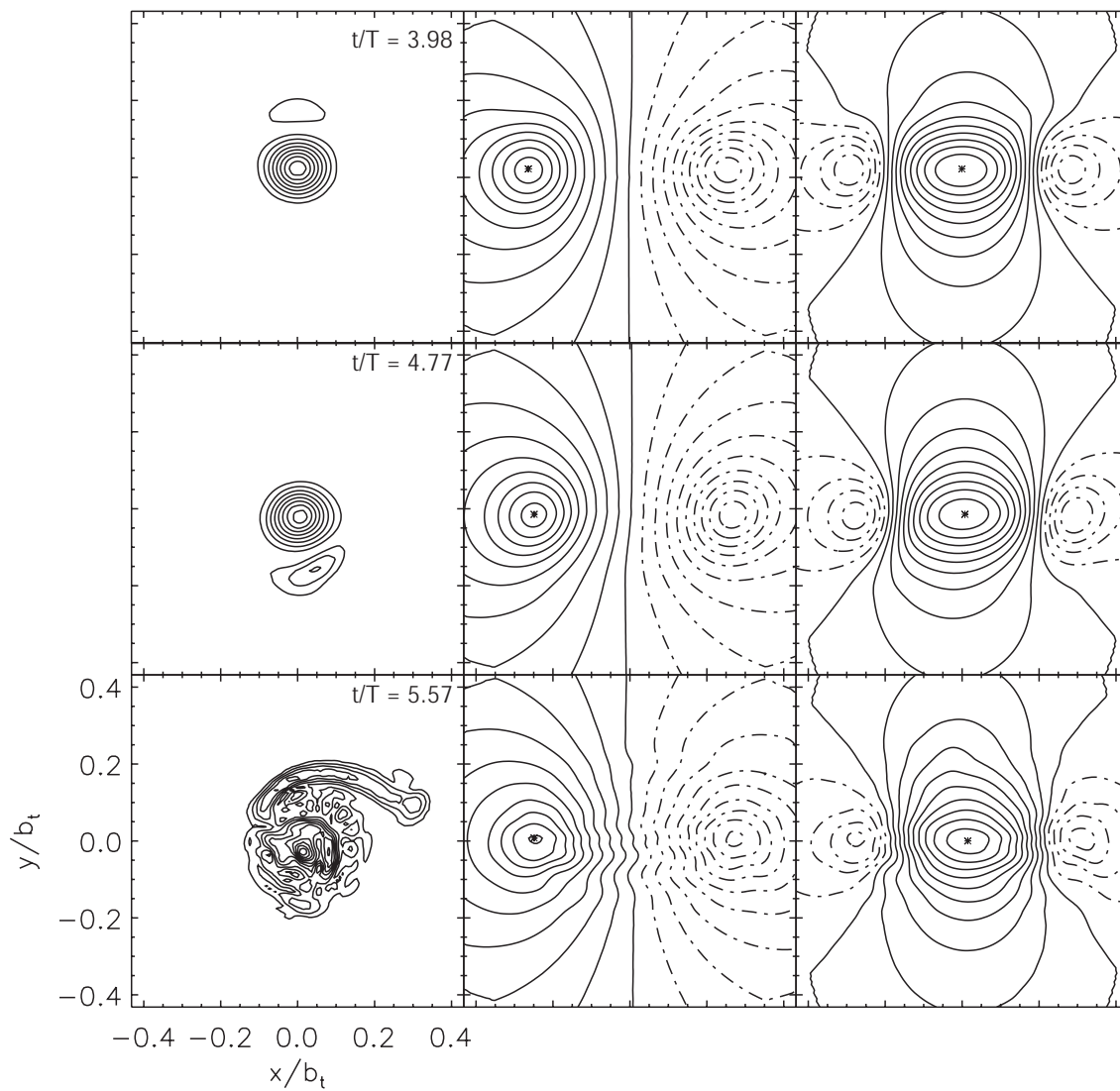
Figure 14. Vorticity (left), downwash (center), and rolling moment (right) contours for a two-vortex system with $\Gamma_f/\Gamma_t = -0.20$ and $d/b_t = 0.125$ sampled at plane 4 indicated in Figure 2. The striking similarities to the contours induced by an isolated Lamb-Oseen vortex are clear. Contours are equally-spaced between the absolute values of the initial maximal values.

American Institute of Aeronautics and Astronautics
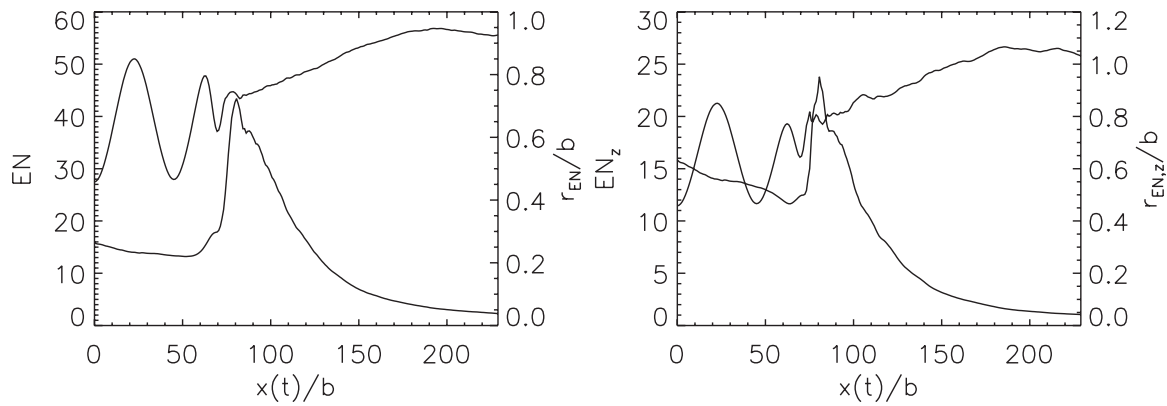
Figure 15. Averaged enstrophy and enstrophy dispersion radius calculations over the full wake from full wake computation: ω^2 (left) and ω_z^2 (right).
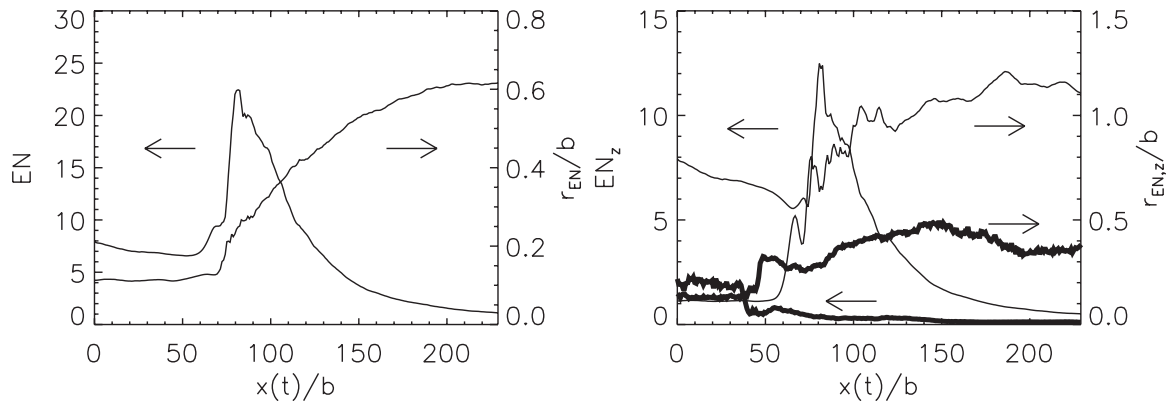
Figure 16. Averaged enstrophy and enstrophy dispersion radius calculations over the half wake from full wake computation and comparisons with experiments (thick lines): ω^2 (left) and ω_z^2 (right). Measurements are from Ortega et al.[5]

American Institute of Aeronautics and Astronautics
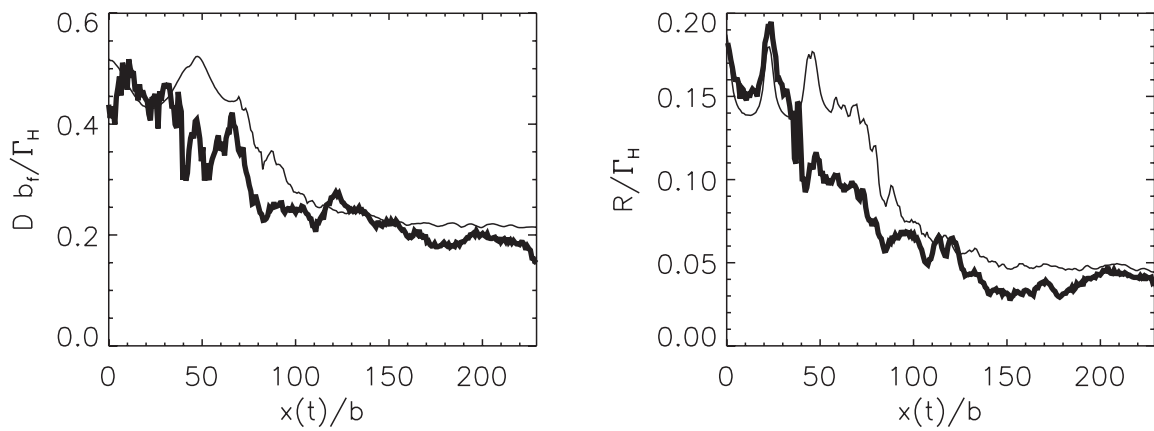
Figure 17. **Comparisons of downwash (left) and rolling moments (right) between measurements (thick lines) and calculations. Measurements are from Ortega et al.[4]**

American Institute of Aeronautics and Astronautics